

Fast Truncated SVD of Sparse and Dense Matrices on Graphics Processors

Andrés E. Tomás*

Enrique S. Quintana-Ortí[†]

Hartwig Anzt[‡]

June 7, 2023

Abstract

We investigate the solution of low-rank matrix approximation problems using the truncated SVD. For this purpose, we develop and optimize GPU implementations for the randomized SVD and a blocked variant of the Lanczos approach. Our work takes advantage of the fact that the two methods are composed of very similar linear algebra building blocks, which can be assembled using numerical kernels from existing high-performance linear algebra libraries. Furthermore, the experiments with several sparse matrices arising in representative real-world applications and synthetic dense test matrices reveal a performance advantage of the block Lanczos algorithm when targeting the same approximation accuracy.

1 Introduction

In data science, dimensionality reduction via low-rank matrix approximation is gaining increasing relevance, for example, in order to pre-process large volumes of information prior to the application of machine learning techniques for data synthesis. In this line, the *singular value decomposition* (SVD) is an important low-rank matrix approximation technique, well-known in numerical linear algebra and scientific computing [8].

The conventional methods for computing the SVD are quite expensive in terms of floating point arithmetic operations (flops). For this reason, a number of alternative algorithms have been proposed over the past few years to obtain a low-rank matrix approximation with a more reduced cost [11, 13, 12, 15]. Some of these meth-

ods present the additional property that the accuracy of the approximation can be adjusted by the user.

In this paper, we address the efficient computation of low-rank matrix approximations via the computation of a truncated SVD, with a special focus on numerical reliability and high performance, making the following specific contributions:

- We develop an implementation of the randomized SVD method introduced in [11], casting its major operations in terms of linear algebra building blocks that are especially appropriate for data-parallel hardware accelerators such as graphics processing units (GPUs).
- In addition, we investigate and implement an alternative for the truncated SVD based on the block Lanczos method [9]. In doing so, we demonstrate that this approach can be decomposed into a collection of linear algebra building blocks very similar to those in our implementation of the randomized SVD algorithm and, therefore, also appropriate for GPUs.
- We provide a complete numerical evaluation of the two types of methods, using a collection of sparse matrices from the Suite Sparse Matrix Collection [4].
At this point, we note that the methods targeted in this work are appropriate for both sparse and dense matrices yet the former type of problem is especially interesting. This is possible because, in both types of methods, the problem matrix remains unmodified, participating only as an input operand to matrix multiplications.
- Finally, we complete the experimental analysis of the methods with a detailed performance evaluation on an NVIDIA Ampere A100 graphics processor.

*Universitat Politècnica de València, Spain.

Corresponding author's email address: antodo@upv.es.

[†]Universitat Politècnica de València, Spain.

[‡]Karlsruhe Institute of Technology, Germany; and Innovative Computing Laboratory, University of Tennessee at Knoxville, USA

The rest of the paper is structured as follows. First, we briefly review the SVD, its use as a tool for obtaining low-rank approximations, and the two algorithms we consider for this operation. We then describe in detail the building blocks in these algorithms, and how to customize them for GPUs. We then evaluate the resulting data-parallel realizations of the algorithms, from the viewpoints of both numerical accuracy and high performance. We finally close the paper with some concluding remarks and a discussion of future work.

2 Truncated SVD

Consider the matrix $A \in \mathbb{R}^{m \times n}$ where, without loss of generality, hereafter we assume that $m \geq n$. (Otherwise, we simply target the transpose of A .) The SVD of the matrix is then given by

$$A = U\Sigma V^T, \quad (1)$$

where $\Sigma = \text{diag}(\sigma_1, \sigma_2, \dots, \sigma_n) \in \mathbb{R}^{m \times n}$ is a diagonal matrix containing the singular values of A , while $U \in \mathbb{R}^{m \times m}$ and $V \in \mathbb{R}^{n \times n}$ are orthogonal matrices with their columns respectively corresponding to the left and right singular vectors of the matrix [8].

In many applications, we are interested in obtaining a *truncated SVD*, of a certain order r , so that

$$U_{\top} \Sigma_{\top} V_{\top}^T \approx A, \quad (2)$$

$\Sigma_{\top} = \text{diag}(\sigma_1, \sigma_2, \dots, \sigma_r) \in \mathbb{R}^{r \times r}$, and U_{\top}, V_{\top} contain the first r columns of U, V , respectively. The practical problem then becomes how to obtain this approximation of A without “paying the price” of computing the full decomposition in (1), which can be considerably higher. This is especially the case when the objective is to obtain a low-rank matrix approximation, for which $r \ll n$.

We close this short review of the truncated SVD by noting that, in some cases, the parameter r is not known in advance, but instead has to be determined based on a user-defined threshold on the difference

$$\|A - U_{\top} \Sigma_{\top} V_{\top}^T\|_2 \approx \sigma_{r+1}, \quad (3)$$

where $\|\cdot\|_2$ denotes the matrix 2-norm. This leads to the interesting problem of constructing an incremental truncated SVD using, for example, an incremental version of the QR factorization [10].

In the remainder of this section, we review two efficient algorithms to compute a truncated SVD: The

Algorithm 1. RandSVD: Truncated SVD via randomized subspace iteration.

Input: $A \in \mathbb{R}^{m \times n}$; parameters $r \in [1, n]$ and $p, b \geq 1$
Output: $U_{\top} \in \mathbb{R}^{m \times r}, \Sigma_{\top} = \text{diag}(\sigma_1, \sigma_2, \dots, \sigma_r),$
 $V_{\top} \in \mathbb{R}^{n \times r}$

Generate a random matrix $Q_0 \in \mathbb{R}^{n \times r}$
for $j = 1, 2, \dots, p$
S1. $\bar{Y}_j = A Q_{j-1}$
S2. Factorize $\bar{Y}_j = \bar{Q}_j \bar{R}_j$ (Alg. 3)
S3. $Y_j = A^T \bar{Q}_j$
S4. Factorize $Y_j = Q_j R_j$ (Alg. 3)
endfor
S5. Factorize $R_p = \bar{U} \Sigma_{\top} \bar{V}^T$ (SVD)
S6. $U_{\top} = \bar{Q}_p \bar{V}$
S7. $V_{\top} = Q_p \bar{U}$

randomized SVD and the block Lanczos-based SVD. These two types can be decomposed into a common collection of basic building blocks for matrix factorizations (Cholesky, QR, SVD), orthogonalization procedures, and matrix multiplications as described in the next section.

2.1 Randomized SVD

Overview. The randomized method for the truncated SVD was originally presented by [13] and can be derived from Algorithm 1 by setting $p = 1$. The idea was subsequently refined in [11] by adding the subspace iteration to the procedure (loop indexed by p), yielding the RandSVD algorithm shown there.

In order to hint why RandSVD delivers a truncated decomposition, consider the last iteration of the loop, where $j = p$. Combining steps S3 and S4, we have that

$$A^T \bar{Q}_p = Q_p R_p. \quad (4)$$

Therefore, transposing both sides of the expression and multiplying them on the left by \bar{Q}_p ,

$$A \approx \bar{Q}_p R_p^T Q_p^T. \quad (5)$$

Finally, taking into account the SVD in step S5, we obtain that

$$\begin{aligned} A &\approx \bar{Q}_p (\bar{U} \Sigma_{\top} \bar{V}^T)^T Q_p^T \\ &= (\bar{Q}_p \bar{V}) \Sigma_{\top} (\bar{U}^T Q_p^T) \\ &= U_{\top} \Sigma_{\top} V_{\top}^T \end{aligned} \quad (6)$$

offers the sought-after low-rank matrix approximation.

Building blocks. From a practical point of view, RandSVD comprises a number of matrix multiplications, two QR factorizations, and an SVD. We make the following observations with respect to these operations:

- For low-rank matrix approximation problems, $r \ll m, n$. When A is a dense matrix, most of the arithmetic corresponds to the matrix multiplications involving A (steps S1 and S3). The method is suitable for sparse problems because during the iteration A is not modified and, therefore, maintains its sparse structure.
- Both QR factorizations involve “tall-and-skinny” matrices, respectively of dimensions $m \times r$ (step S2) and $n \times r$ (step S4). Our realization of these factorizations, to be presented in the next section, constructs the Q_j and \tilde{Q}_j explicitly.
- After the loop, the SVD (step S5) operates with a very small ($r \times r$) matrix. The computational cost of this operation is hence negligible.
- Finally, with the matrices in the sequences Q_j and \tilde{Q}_j explicitly built, the iteration requires two additional matrix multiplications after the loop (steps S6 and S7).

Role of the parameters p and r . The original RandSVD is formulated in our case as a direct method where $p = 1$. However, this approach may compute very poor approximations of the singular values unless they are well separated. By setting $p > 1$, the method performs $p - 1$ subspace iterations, gradually improving the accuracy of the computed singular values. In general, a larger value for p delivers more accurate approximations. However, as the algorithm exposes, the computational cost increases linearly with p .

The parameter r controls the number of vectors in the subspace iteration and should at least equal the number of singular values that are required. Typically, p is set to a handful of vectors more than the number of singular values to compute.

2.2 Block Lanczos SVD

Overview. Algorithm 2 presents the LancSVD procedure for the truncated SVD based on the block Golub-Kahan-Lanczos method [9], with the block size parameterized by b . (For simplicity, we assume that r is an integer multiple of b .) The LancSVD algorithm there is

formulated with a fixed number of iterations, in order to expose the similarities and differences with RandSVD.

Starting with a random orthonormal matrix $\tilde{P}_1 \in \mathbb{R}^{m \times b}$, at iteration k LancSVD builds two matrices, $P_k \in \mathbb{R}^{n \times r}$ and $\tilde{P}_k \in \mathbb{R}^{m \times r}$, such that

$$\begin{aligned} A^T \tilde{P}_k &= P_k B_k, \quad \text{and} \\ AP_k &= \tilde{P}_k B_k + \tilde{Q}_{k+1} R_k E_k, \end{aligned} \quad (7)$$

where P_k and \tilde{P}_k have orthonormal columns, (that is, $P_k^T P_k = \tilde{P}_k^T \tilde{P}_k = I$, where I denotes the identity matrix of the appropriate order), and $\tilde{P}_k^T \tilde{Q}_{k+1} = I$. Furthermore, E_k denotes the last r columns of an identity matrix of the appropriate order; and $B_k \in \mathbb{R}^{r \times r}$ is a lower triangular matrix with b non-zero diagonals below the main diagonal and the following structure:

$$B_k = \begin{bmatrix} L_1 & & & & & \\ R_1 & L_2 & & & & \\ & R_2 & \ddots & & & \\ & & \ddots & L_{k-1} & & \\ & & & R_{k-1} & L_k & \end{bmatrix}, \quad (8)$$

where R_i and L_i are respectively upper and lower triangular matrices of order $b \times b$.

If the norm of R_k is small, the singular values of B_k approximate the largest k singular values of A . Replacing B_k by its SVD decomposition

$$B_k = \tilde{U} \Sigma \tilde{V}^T, \quad (9)$$

we thus obtain

$$AP_k = \tilde{P}_k B_k + \tilde{Q}_{k+1} R_k E_k, \quad (10)$$

so that

$$\begin{aligned} A &= \tilde{P}_k B_k P_k^T + \tilde{Q}_{k+1} R_k E_k P_k^T, \\ &\approx \tilde{P}_k B_k P_k^T = \tilde{P}_k U \Sigma \tilde{V}^T P_k^T. \end{aligned} \quad (11)$$

The previous equations show also that the left and right singular vectors of A can be obtained from the Lanczos vectors and singular vectors of B_k as follows:

$$U = \tilde{P}_k \tilde{U}, \quad V = P_k \tilde{V}. \quad (12)$$

It is well known that the original Lanczos algorithm implemented in floating point arithmetic fails to compute fully orthogonal matrices. From the multiple solutions proposed in the literature, we choose the full orthogonalization against all previous Lanczos vectors. This approach is computationally expensive, but it

Algorithm 2. LancSVD: Truncated SVD via block Lanczos method with one-side full orthogonalization and basic restart.

<p>Input: $A \in \mathbb{R}^{m \times n}$; parameters $r \in [1, n]$; $p, b \geq 1$ Output: $U_{\top} \in \mathbb{R}^{m \times r}, \Sigma_{\top} = \text{diag}(\sigma_1, \sigma_2, \dots, \sigma_r),$ $V_{\top} \in \mathbb{R}^{n \times r}$</p> <p>S1. Generate a random orthonormal matrix $\tilde{Q}_1 \in \mathbb{R}^{m \times b}$ (Alg. 4) $k = r/b$ for $j = 1, 2, \dots, p$ for $i = 1, 2, \dots, k$</p> <p>S2. $Q_i = A^T \tilde{Q}_i$ if $i == 1$</p> <p>S3a. Orthogonalize Q_1 obtaining L_1^T (Alg. 4) else</p> <p>S3b. Orthogonalize Q_i against $P_{i-1} = [Q_1 Q_2 \dots Q_{i-1}]$ obtaining H_i and L_i^T (Alg. 5) endif</p> <p>S4. $\tilde{Q}_{i+1} = A Q_i$</p> <p>S5. Orthogonalize \tilde{Q}_{i+1} against $\tilde{P}_i = [\tilde{Q}_1 \tilde{Q}_2 \dots \tilde{Q}_i]$ obtaining \tilde{H}_i and R_i (Alg. 5) endfor</p> <p>S6. Factorize $B_k = \tilde{U} \Sigma_{\top} \tilde{V}^T$ (SVD) if $j < p$ Split $\tilde{U} \rightarrow [\tilde{U}_1 \tilde{U}_2 \dots \tilde{U}_k]$</p> <p>S7. $\tilde{Q}_1 = [\tilde{Q}_1 \tilde{Q}_2 \dots \tilde{Q}_k] \tilde{U}_1$ endif endfor</p> <p>S8. $V_{\top} = [Q_1 Q_2 \dots Q_k] \tilde{V}^T$</p> <p>S9. $U_{\top} = [\tilde{Q}_1 \tilde{Q}_2 \dots \tilde{Q}_k] \tilde{U}$</p>

presents the advantage of being composed of large matrix operations, which are very efficient to compute in GPUs.

The main drawback of the full orthogonalization approach is that the computational cost of the Lanczos method rapidly increases with the number of iterations, as each iteration adds new columns to the basis that has to be employed in the orthogonalization. Also, the amount of memory to store all the previous Lanczos vectors grows linearly. In order to avoid these issues, a restarting technique is frequently used in combination with the Lanczos method. There are several restarting techniques in the literature, see for example [2], but for simplicity we choose the original one from [9]. In

this approach, the Lanczos iteration is also run several times, but instead of using random vectors as the initial vectors after each restart, these are set to the approximations of the left singular vectors associated with the b largest singular values. As a result, the new Lanczos iteration maintains the most relevant part of the search directions computed in the previous iteration.

Building blocks. We identify the following components in LancSVD, with a significant intersection with those present in RandSVD as well as a few differences:

- The algorithm comprises matrix multiplications with A^T and A (steps S2, S4, respectively). When A is dense, for low-approximation problems, the arithmetic cost is dominated by these matrix multiplications. The algorithm is also appropriate for sparse problems, since A is not modified during the computations.
- The algorithm performs three orthogonalizations (steps S1, S3a/S3b, S4). In the next section we will show that the methods for these are akin in our case to that employed for the QR factorization present in RandSVD.
- In the loop there is a small SVD, of size $r \times r$, (step S5) with a negligible computational cost.
- Assuming the matrices Q_1, Q_2, \dots, Q_k and $\tilde{Q}_1, \tilde{Q}_2, \dots, \tilde{Q}_k$ are explicitly built, there are two additional matrix multiplications after the loop (steps S8, S9).

Role of the parameter b . Choosing a moderate blocking size b makes the matrix multiplications in steps S2, S4 and the orthogonalization in steps S1, S3, S5 more efficient. Typically, the optimal value for this parameter depends on the hardware architecture, with the performance initially increasing as it grows, but with a point from which the operations do not become any faster.

Furthermore, b should be chosen as large as the number of desired singular values/vectors for maximum effectiveness of the restarting procedure. In this way, a Lanczos vector is preserved for each wanted singular triplet and it is improved at each restart.

Role of the parameter r . This parameter controls the size of the Krylov subspace generated by LancSVD. A

large value of r improves the convergence, but the cost of the orthogonalization grows at a faster-than-linear pace with it. Also, a large amount of memory is required to store all the generated Lanczos vectors. The convergence rate of the Lanczos procedure mostly depends on the number of matrix applications, which is determined by the ratio $k = r/b$. When $b = 1$, LancSVD becomes the single vector Lanczos iteration with the best convergence rate, but the implementation may be less efficient on a current architecture.

Role of the parameter p . This parameter allows to continue the Lanczos iteration without incurring in the extra costs of a large r . In a practical implementation of the algorithm, b is set depending on the hardware, r is set taking into account the computation and memory costs, and p is increased till the approximations to the singular triplets satisfy the desired accuracy.

3 Building Blocks on GPUs

In this section we provide a high level algorithmic description of our realizations of the main building blocks identified during the presentation of the RandSVD and LancSVD algorithms. In addition, we motivate the selection of the particular realizations chosen for these building blocks, and we connect (most of) them with high performance implementations of these operations in current linear algebra libraries for massively data-parallel graphics processors.

3.1 QR factorization via block Gram-Schmidt

The loop indexed by j in RandSVD (see Algorithm 1) comprises the QR factorizations of two tall-and-skinny matrices per iteration. These decompositions can be computed, for example, using the conventional, block column-oriented formulation based on Householder transforms. Alternatively, due to the dimension of the matrices, it may be more efficient to employ a communication-avoiding algorithm for the QR factorization (CAQR) that increases the degree of parallelism [8, 5, 1].

In our case, given that the target architecture is a GPU and, the triangular factors resulting from the QR factorizations in the sequences for Y_j and \bar{Y}_j are not needed (except for the last one), we decided to compute the factorizations in RandSVD using a blocked variant of the

Algorithm 3. CGS-QR: QR factorization via block Gram-Schmidt.

Input: $Y \in \mathbb{R}^{q \times r}$; parameter $b \geq 1$
Output: $Q \in \mathbb{R}^{q \times r}$, $R \in \mathbb{R}^{r \times r}$

$k = r/b$
 $Q = Y$, partitioned by column blocks as
 $Q \rightarrow [Q_1 Q_2 \dots Q_k]$

S1. Orthogonalize Q_1 obtaining R_1 (Alg. 4)
for $j = 2, 3, \dots, k$

S2. Orthogonalize Q_j against $P_{j-1} = [Q_1 Q_2 \dots Q_{j-1}]$
obtaining H_j and R_j (Alg. 5)
Assemble $R_j \leftarrow \begin{bmatrix} H_j \\ R_j \end{bmatrix}$

endfor
Assemble R by column blocks, $R \leftarrow [R_1 R_2 \dots R_k]$

classical Gram-Schmidt (CGS) method; see [3]. This algorithm is simple to implement on GPUs; it is composed of highly efficient building blocks for this type of data-parallel hardware accelerators; and it provides a numerical accuracy similar to that of conventional methods for the QR factorization for about the same arithmetic cost.

Algorithm 3 sketches the CGS-QR algorithm for the QR factorization. When called from Algorithm 1 to factorize the sequence Y_j , the dimension $q = m$. For the sequence \bar{Y}_j , $q = n$. The algorithm basically invokes an orthogonalization procedure (steps S1, S2), using a method to be discussed in the final part of this section. The remaining operations in the algorithm involve partitioning and data movements but no relevant arithmetic.

3.2 Orthogonalization via CholeskyQR2

For the orthogonalization procedures required in LancSVD and CGS-QR (see Algorithms 2 and 3, respectively), we decided to implement a GPU version of the CholeskyQR2 algorithm [6]. In this approach, the procedure is repeated twice to ensure the orthogonality of the resulting factor Q . In case of a breakdown in the Cholesky decomposition the implementation reverts to a classical Gram-Schmidt with re-orthogonalization.

Algorithm 4 shows the CholeskyQR2 orthogonalization procedure. There, $q = m$ or $q = n$, depending on the operation of the algorithm that utilizes it. The procedure consists of a few basic linear algebra building blocks such as matrix multiplications (steps S1, S4,

Algorithm 4. CholeskyQR2: Orthogonalization.

Input: $Q \in \mathbb{R}^{q \times b}$
Output: $Q \in \mathbb{R}^{q \times b}, R \in \mathbb{R}^{b \times b}$

S1. $W = Q^T Q$
S2. Factorize $W = LL^T$ (Cholesky factorization)
S3. $\bar{Q} = QL^{-T}$
S4. $\bar{W} = \bar{Q}^T \bar{Q}$
S5. Factorize $\bar{W} = \bar{L}\bar{L}^T$ (Cholesky factorization)
S6. $Q = Q\bar{L}^{-T}$
S7. $R = \bar{L}^T \bar{L}^T$

S7); triangular system solves (steps S3, S6); and two Cholesky factorizations (steps S2, S5); see [8].

3.3 Orthogonalization via CGS and CholeskyQR2

The complementary orthogonalization procedure, required by LancSVD and CGS-QR, is implemented using a combination of block classical Gram-Schmidt and CholeskyQR2. As in the case of the latter, the orthogonalization procedure performs a second pass, in order to improve the numerical stability of the solution [7].

Algorithm 5 shows the details of this orthogonalization procedure. When this procedure is called from CGS-QR, the dimension $q = m$ or $q = n$. In both cases, when invoked at iteration j of the corresponding algorithm, the dimension $s = (j - 1)b$. The main building blocks in the procedure are the same as those already identified for CholeskyQR2: Matrix multiplications (steps S1, S2, S3, S6, S7, S8, S11); triangular system solves (steps S5, S10); and two Cholesky factorizations (steps S4, S9). There is only one different operation, matrix addition (step S12), but this contributes a negligible computational cost.

3.4 Building blocks, high performance libraries, and computational cost

Our realizations of RandSVD and LancSVD are composed of several basic linear algebra operations such as matrix multiplications in various forms (sparse, general, triangular) and triangular system solves, plus two elaborate matrix factorizations (SVD and Cholesky). To perform the basic operations, we rely on routines from high performance linear algebra libraries for GPUs: cuSPARSE (for sparse matrix multiplications) and cuBLAS

Algorithm 5. CGS-CQR2: Orthogonalization via CGS and CholeskyQR2.

Input: $Q \in \mathbb{R}^{q \times b}, P \in \mathbb{R}^{q \times s}$
Output: $Q \in \mathbb{R}^{q \times b}, H \in \mathbb{R}^{s \times b}, R \in \mathbb{R}^{b \times b}$

S1. $H = P^T Q$
S2. $Q = Q - PH$
S3. $W = Q^T Q$
S4. Factorize $W = LL^T$ (Cholesky factorization)
S5. $\bar{Q} = QL^{-T}$
S6. $\bar{H} = P^T \bar{Q}$
S7. $Q = Q - P\bar{H}$
S8. $W = Q^T Q$
S9. Factorize $W = \bar{L}\bar{L}^T$ (Cholesky factorization)
S10. $Q = Q\bar{L}^{-T}$
S11. $R = \bar{L}^T \bar{L}^T$
S12. $H = H + \bar{H}$

(for dense and triangular operations). In the case of the matrix factorizations, due to their complexity and the small dimension of their input operands, we instead rely on LAPACK to compute them on the CPU.

Table 1 specifies 1) the routines employed for the operation at each step of the algorithms and building blocks; 2) the libraries they belong to; 3) the target architecture (GPU, CPU or hybrid); 4) their theoretical costs (in floating point operations, or flops); and 5) the matrix transfers between CPU and GPU. The total costs, also reported there, can be derived from the expressions in the table. For example, the cost of RandSVD is obtained by adding the cost of steps S1–S4 multiplied by the number of iterations of the algorithm loop (p), and next adding also the cost of steps S5–S7. In this case, CA3 (acronym for cost of Alg. 3) is a function that returns the cost of CholeskyQR2 when invoked with $r = b$ and either $q = m$ (for step S2) or $q = m$ (for step S4). Similarly, the cost of CGS-QR is given by

$$CA4(b, q) + \sum_{j=2}^{r/b} CA5(b, q, s), \quad (13)$$

where CA4, CA5 (for cost of Algs. 4, 5) are functions that respectively return the cost of CholeskyQR2 and the cost of CGS-CQR2 when invoked at iteration j with $s = (j - 1)b$.

Table 1 exposes that the computational cost of the truncated SVD algorithm depends on the problem dimensions (m, n and, for sparse problems, the number of

Table 1. Algorithms and building blocks considering A is a sparse matrix with n_z nonzero entries. In case the matrix is dense, the operations with the “*” superscript are performed on the GPU using routine GEMM from cuBLAS, and their cost becomes $2mnr$. In the cost expressions, CA3, CA4, CA5 return the cost of algorithms 3 (CGS-QR), 4 (CholeskyQR2) and 5 (CGS-CQR2) as a function of their input parameters. CS1, CS2, CS3, ... refer to the costs of the individual steps.

Algorithm	Step	Algorithm/ routine	Library	Target	Cost	Matrix transfers
Alg. 1 RandSVD	S1	SpMM*	cuSPARSE	GPU	$2n_z r$	
	S2	Alg. 3	–	Hybrid	$CA3(b, m, r)$	
	S3	SpMM*	cuSPARSE	GPU	$2n_z r$	
	S4	Alg. 3	–	Hybrid	$CA3(b, n, r)$	
	S5	GESVD	LAPACK	CPU	$O(r^3)$	Transfer R_p GPU→CPU
	S6	GEMM	cuBLAS	GPU	$2mr^2$	Transfer \tilde{V} CPU→GPU
	S7	GEMM	cuBLAS	GPU	$2nr^2$	Transfer \tilde{U} CPU→GPU
Total cost	$p \left[CS1 + CA3(b, m, r) + CS3 + CA3(b, n, r) \right] + CS5 + CS6 + CS7$					
Alg. 2 LancSVD	S1	Alg. 4	–	Hybrid	$CA4(b, m)$	
	S2	SpMM*	cuSPARSE	GPU	$2n_z b$	
	S3a	Alg. 4	–	Hybrid	$CA4(b, n)$	
	S3b	Alg. 5	–	Hybrid	$CA5(b, n, s = (i - 1)b)$	
	S4	SpMM*	cuSPARSE	GPU	$2n_z b$	
	S5	Alg. 5	–	Hybrid	$CA5(b, m, s = ib)$	
	S6	GESVD	LAPACK	CPU	$O(r^3)$	Transfer B GPU→CPU
	S7	GEMM	cuBLAS	GPU	$2bmr$	Transfer \tilde{U}_1 CPU→GPU
	S8	GEMM	cuBLAS	GPU	$2nr^2$	Transfer \tilde{V} CPU→GPU
S9	GEMM	cuBLAS	GPU	$2mr^2$	Transfer \tilde{U} CPU→GPU	
Total cost	$CS1 + \sum_{j=1}^p \left[\sum_{i=1}^{r/b} \left[CS2 + CS3 + CS4 + CA5(b, m, ib) \right] + CS6 + CS7 \right] + CS8 + CS9$ If $i == 1$, $CS3 = CA4(b, n)$ else $CS3 = CA5(b, n, (i - 1)b)$ If $j < p$, $CS7 = 2bmr$ else $CS7 = 0$					
Alg. 3 CGS-QR	S1	Alg. 4	–	Hybrid	$CA4(b, q)$	
	S2	Alg. 5	–	Hybrid	$CA5(b, q, s = (j - 1)b)$	
Total cost	$CA4(b, q) + \sum_{j=2}^{r/b} CA5(b, q, (j - 1)b)$					
Alg. 4 CholeskyQR2	S1/S4	GEMM	cuBLAS	GPU	$b^2 q$	
	S2/S5	POTRF	LAPACK	CPU	$b^3/3$	Transfer W GPU→CPU
	S3/S6	TRSM	cuBLAS	GPU	$b^2 q$	Transfer L CPU→GPU
	S7	TRMM	BLAS	CPU	b^3	
Total cost	$CS1 + CS2 + \dots + CS7$					
Alg. 5 CGS-CQR2	S1/S6	GEMM	cuBLAS	GPU	$2bqs$	
	S2/S7	GEMM	cuBLAS	GPU	$2bqs$	
	S3/S8	GEMM	cuBLAS	GPU	$2b^2 q$	
	S4/S9	POTRF	LAPACK	GPU	$b^3/3$	Transfer W GPU→CPU
	S5/S10	TRSM	cuBLAS	GPU	$b^2 q$	Transfer L CPU→GPU
	S11	TRMM	BLAS	CPU	b^3	
	S12	ADD	Custom	CPU	bs	
Total cost	$CS1 + CS2 + \dots + CS12$					

Table 2. Matrices used in the experiments.

Matrix	Rows	Columns	n_z	Matrix	Rows	Columns	n_z
12month1	12 471	872 622	22 624 727	ch7-9-b4	317 520	105 840	1 587 600
ch8-8-b4	376 320	117 600	1 881 600	connectus	512	394 792	1 127 525
dbic1	43 200	226 317	1 081 843	degme	185 501	659 415	8 127 528
Delor295K	295 734	1 823 928	2 401 323	Delor338K	343 236	887 058	4 211 599
Delor64K	64 719	1 785 345	652 140	ESOC	327 062	37 830	6 019 939
EternityII.E	11 077	262 144	1 503 732	EternityII_Etilde	10 054	204 304	1 170 516
fome21	67 748	216 350	465 294	GL7d15	460 261	171 375	6 080 381
GL7d16	955 128	460 261	14 488 881	GL7d22	349 443	822 922	8 251 000
GL7d23	105 054	349 443	2 695 430	Hardesty2	929 901	303 645	4 020 731
IMDB	428 440	896 308	3 782 463	LargeRegFile	2 111 154	801 374	4 944 201
lp_nug30	52 260	379 350	1 567 800	lp_osa_60	10 280	243 246	1 408 073
mesh_deform	234 023	9 393	853 829	NotreDame_actors	392 400	127 823	1 470 404
pds-100	156 243	514 577	1 096 002	pds-40	66 844	217 531	466 800
pds-50	83 060	275 814	590 833	pds-60	99 431	336 421	719 557
pds-70	114 944	390 005	833 465	pds-80	129 181	434 580	927 826
pds-90	142 823	475 448	1 014 136	rail2586	2 586	923 269	8 011 362
rail4284	4 284	1 096 894	11 284 032	rel8	345 688	12 347	821 839
rel9	9 888 048	274 669	23 667 183	relat8	345 688	12 347	1 334 038
relat9	12 360 060	549 336	38 955 420	Rucci1	1 977 885	109 900	7 791 168
shar_te2-b2	200 200	17 160	600 600	sls	1 748 122	62 729	6 804 304
spal_004	10 203	321 696	46 168 124	specular	477 976	1 600	7 647 040
stat96v2	29 089	957 432	2 852 184	stat96v3	33 841	1 113 780	3 317 736
stormG2_1000	528 185	1 377 306	3 459 881	tp-6	142 752	1 014 301	11 537 419

non-zero elements n_z) as well as on the algorithmic parameters p , r and b . The expression for the total costs indicate that the relation between p and the cost is linear. However, the impact of r on the cost is more subtle, as discussed next:

- For RandSVD, increasing r will produce linear increments in the cost for steps S1, S3; quadratic for S2, S4, S6, S7; and cubic for S5.
- For the LancSVD, the cost for step S7 grows linearly with r ; quadratically for steps S8, S9; and cubically for step S6. Increasing r has no impact on an individual sparse-general matrix multiplications (SpMM, steps S2 and S4), but the number of them grows linearly with it because we perform r/b operations of this type. Similar reasoning concludes that the costs of (S3a+S3b) and S4 are quadratic on r .

Globally, the impact of r on the total cost is determined by which of these steps dominate, yet this is problem-dependent. Finally, the impact of b on the cost of the two algorithms only affects a few of their steps to a minor extent, and plays no role in the cost of the remaining ones.

4 Experimental results

The experiments in this section were carried out, using IEEE double precision (i.e., 64-bit) arithmetic, on a server equipped with an AMD EPYC 7282 16-core processor (2.8 GHz) and 504 GB of DDR4 memory. In addition, the system is connected via a PCIe bus to an NVIDIA A100 graphics accelerator with 40 GB of DDR5 memory. The platform runs Ubuntu 10.04.6 distribution (Linux Kernel 4.15.0) and the following software: gcc v8.4.0, CUDA Toolkit 11.2 (including the cuBLAS, cuSPARSE, and cuRAND libraries), and Intel MKL 2021.2.0.

As suggested in [13], the initial vectors for RandSVD are generated on the GPU using the cuRAND library with a random Poisson distribution with zero mean and deviation of 1. The initial vectors for LancSVD are generated in the same manner, yet with an orthonormalization afterwards (step S1). All results we report next are averaged over several executions following warm-up runs.

In the experiments, we assume that the objective is to obtain the 10 largest singular values/vectors of the

problem. The accuracy of the computed values will be evaluated using the relative residual

$$\mathcal{R}_j = \|Au_j - \sigma_j v_j\|_2 / \sigma_j, \quad (14)$$

where σ_j , u_j and v_j respectively denote the computed j -th singular value, left singular vector and right singular vector; and $\|\cdot\|_2$ stands for the vector 2-norm. This metric has the advantage of combining the reliability of the singular value and both singular vectors in a single number.

4.1 Sparse problems

For the evaluation of the methods with sparse matrices, we selected several real cases from the Suite Sparse Matrix Collection. In particular, we chose rectangular and large matrices with more than 200 000 rows or columns, and the large dimension being more than two times larger than the short one. Matrices are stored in CSR format, using the default cuSPARSE algorithm, as we experimentally found that this combination is optimal or sufficiently close to the optimal one for all cases.

4.1.1 Accuracy

The discussion at the end of the previous section highlighted the impact of the algorithmic parameters p , r , b on the theoretical cost of RandSVD and LancSVD. We next expose that these parameters exert a key effect on the convergence rate of the algorithms and the accuracy of the computed singular values and vectors.

In order to compute the 10 largest singular values/vectors with LancSVD, we set $b = 16$, $r = 256$, and $p = 2$. That is, we perform $r/b = 256/16 = 16$ Lanczos iterations with $p = 2$ restarts. These parameters were determined experimentally by inspecting the computed relative residuals for different configurations. This is done to compare LancSVD with RandSVD which, in contrast with the former, is presented in the literature as a direct algorithm. In a practical implementation, LancSVD would be formulated as an iterative algorithm where p is increased till the desired accuracy is achieved (within an iteration count limit).

Figure 1 reveals that the residual \mathcal{R}_1 for the solution computed with LancSVD is in the range between 10^{-14} and 10^{-8} ; and between 10^{-14} and 10^{-4} for \mathcal{R}_{10} , except for five cases where the latter lies in the range $[10^{-4}, 10^{-2}]$. In the following, we will consider these accuracy levels as the baseline for the evaluation of the

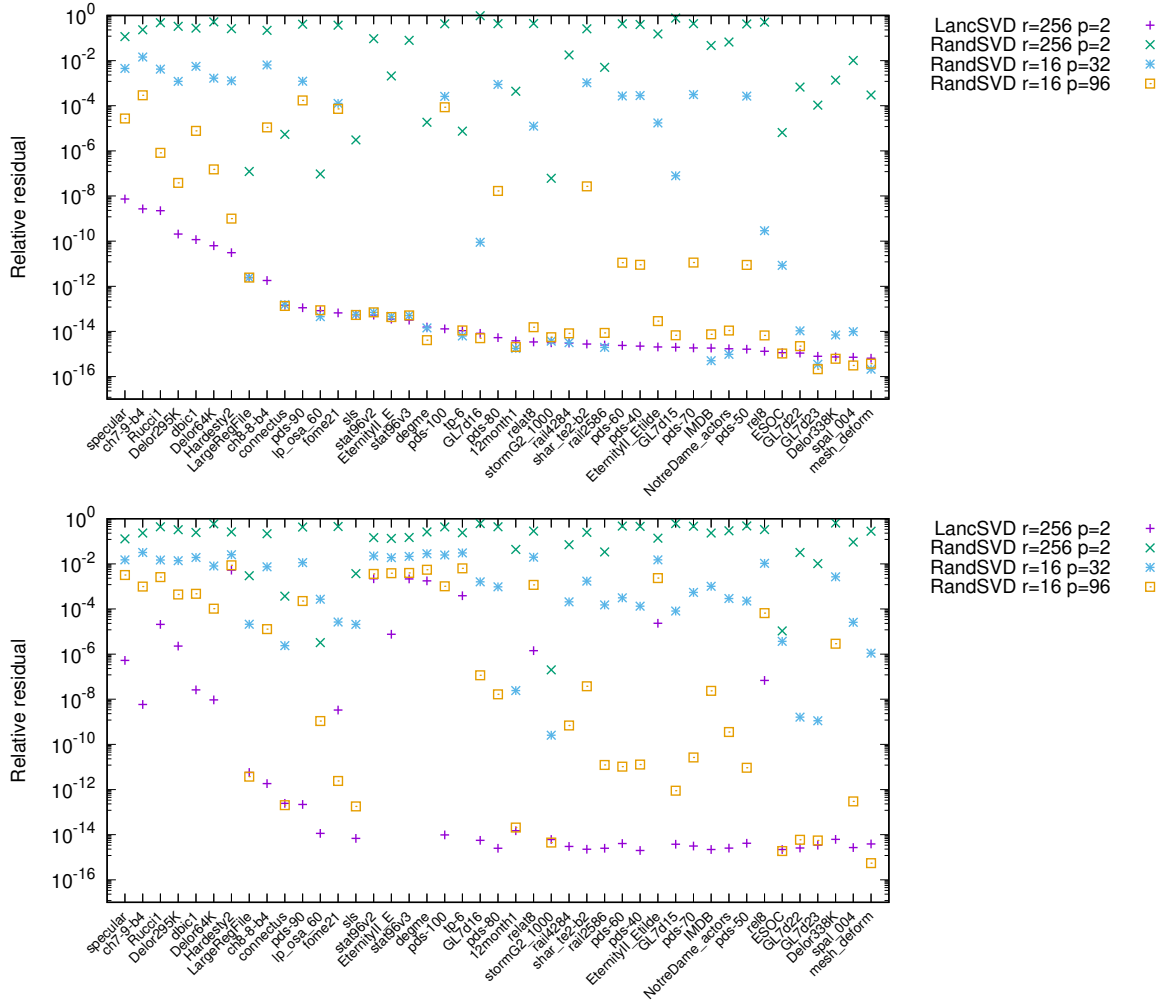


Figure 1. Relative residuals \mathcal{R}_1 (top) and \mathcal{R}_{10} (bottom) for the solutions computed with RandSVD and LancSVD and different values of r and p . In all cases, $b = 16$.

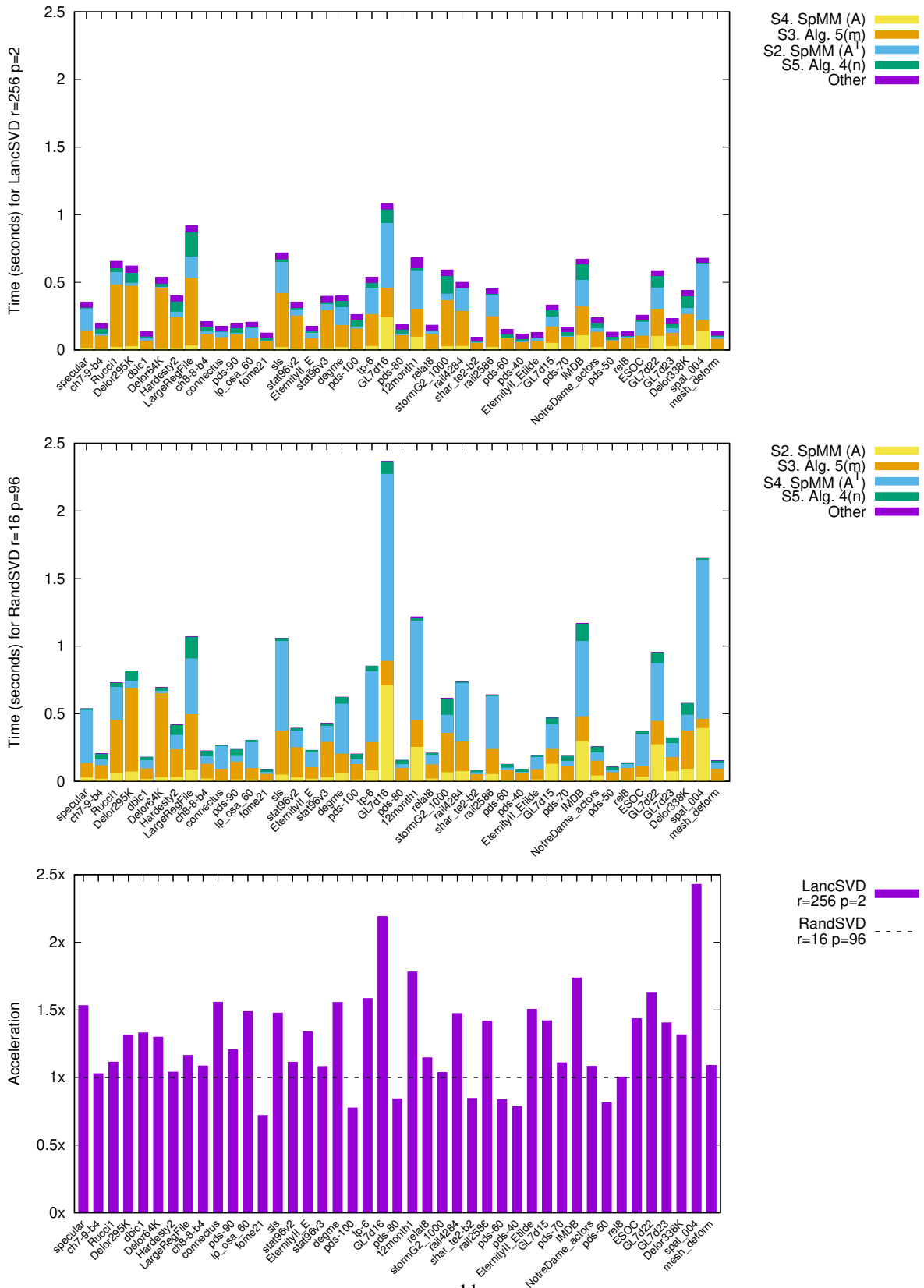


Figure 2. Execution time of LancSVD and RandSVD (top and middle, respectively) and speed-up of LancSVD with respect to RandSVD (bottom).

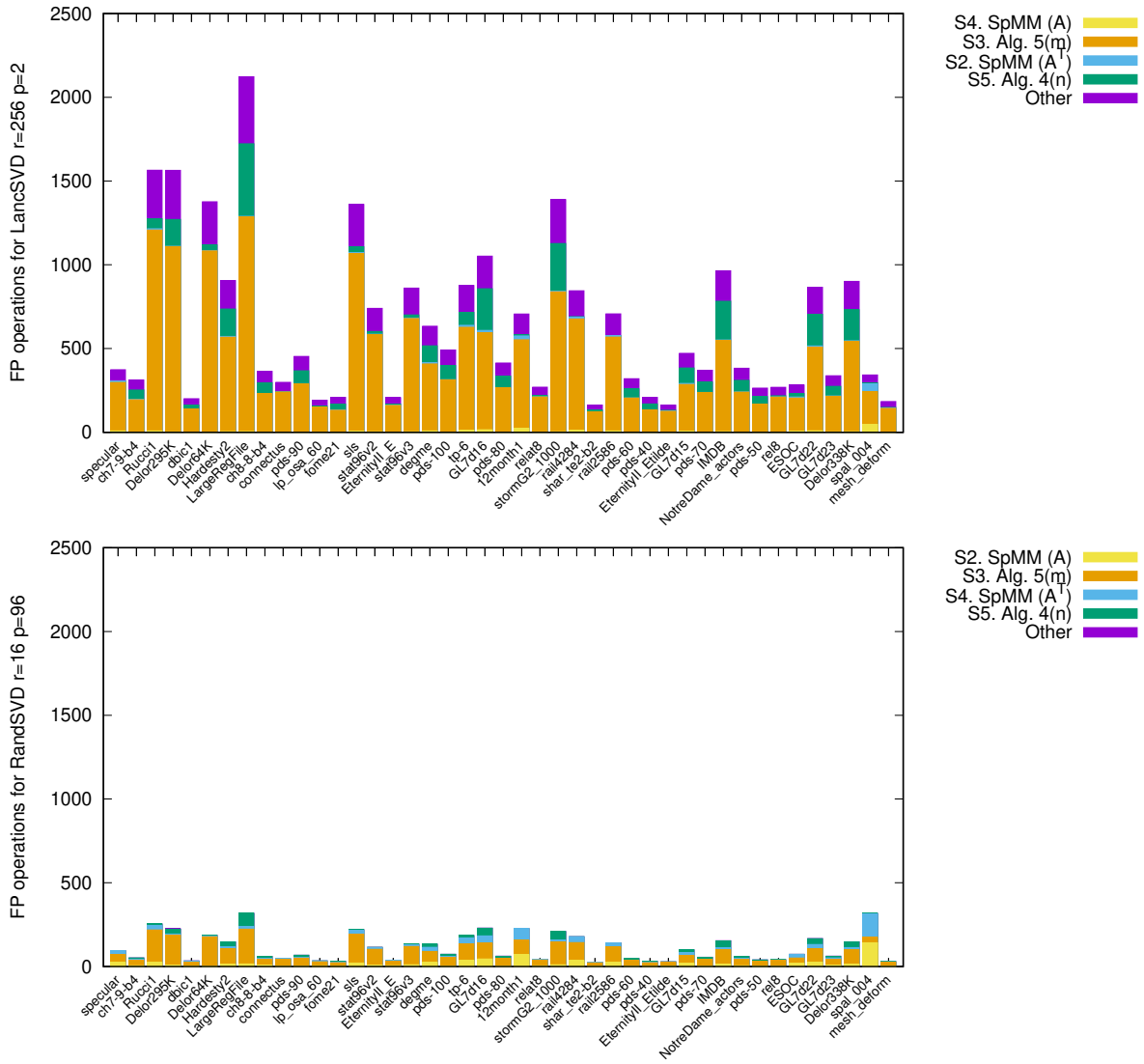


Figure 3. Distribution of the flops across the major building blocks in LancSVD and RandSVD (top and bottom, respectively).

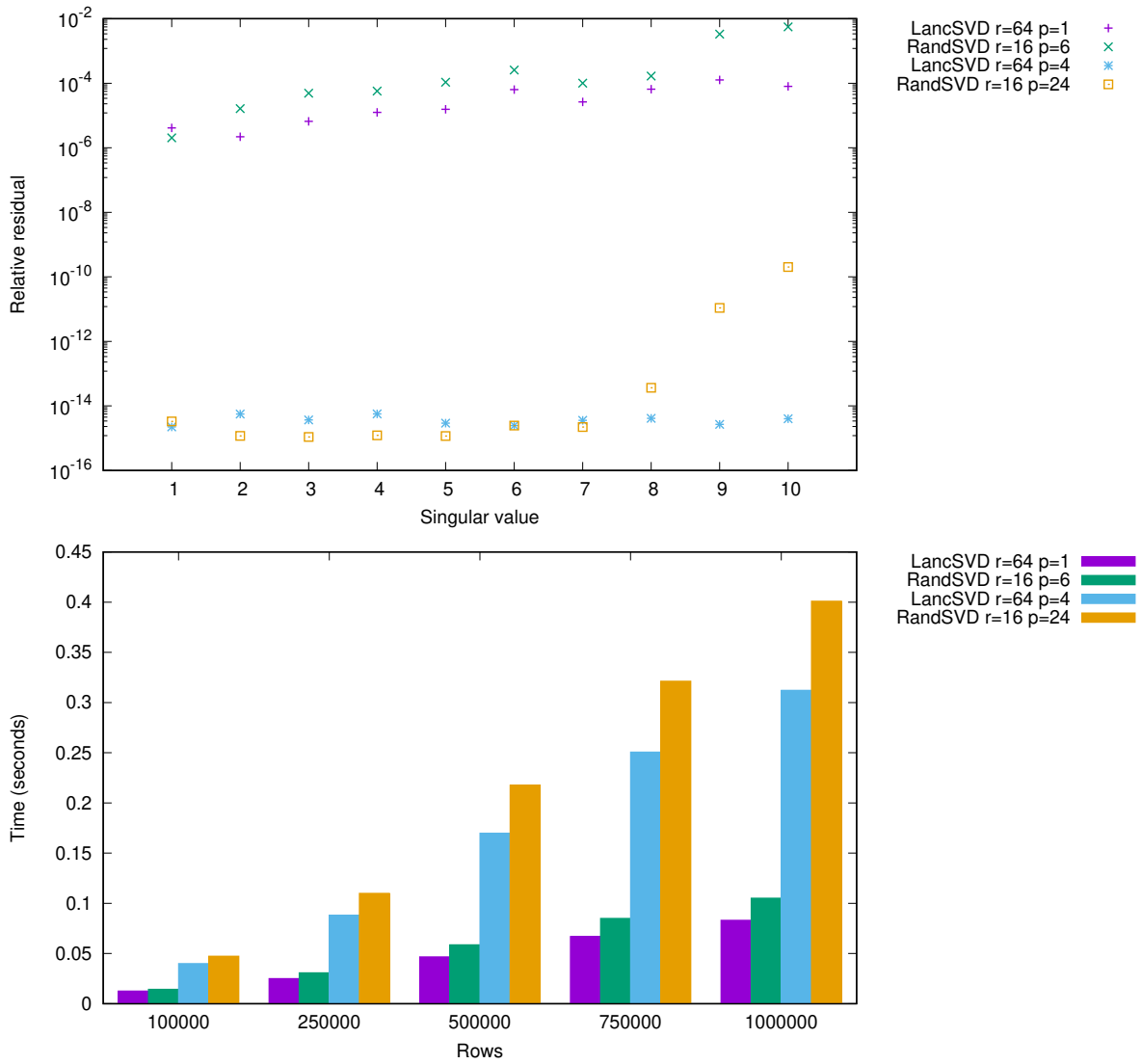


Figure 4. Relative residuals \mathcal{R}_1 to \mathcal{R}_{10} for the solutions computed with the LancSVD and RandSVD and different values of r and p (top) and execution time (bottom). In all cases, $b = 16$.

RandSVD counterpart. For an easy comparison, the results for the sparse problems are ordered according to decreasing values of the metric \mathcal{R}_1 for the solution computed with LancSVD.

Figure 1 also shows the accuracy of the solutions computed with RandSVD for three cases:

1. $r = 256, p = 2$, for which the theoretical cost of RandSVD is similar to that of LancSVD;
2. $r = 16, p = 32$, as this case reduces considerably the theoretical cost of RandSVD compared to that of LancSVD, while maintaining the same number of sparse matrix multiplications;
3. $r = 16, p = 96$, because these tuple offers a residual \mathcal{R}_1 that is close to that attained with LancSVD for about half of the cases.

For all these three configurations, we set $b = 16$.

The quick conclusion from this study is that RandSVD requires a large value of p in order to attain a relative residual that is close to that of the solutions computed with LancSVD. For that reason, we will only consider RandSVD with $r = 16, p = 96$ in the following experiments (and LancSVD with $r = 256, p = 2$). We emphasize that, even with this large value for p , the relative residual of the singular values and vectors computed with RandSVD still lags behind that of LancSVD, with the difference being larger for the smaller singular values/vectors. This difference is due to the convergence properties of RandSVD, which are the same as those of the classic subspace iteration method. In comparison, LancSVD could exhibit super-linear convergence as is common for other Krylov methods [14]. The lesson to take away is that obtaining an accuracy that is close to the baseline set by LancSVD may be prohibitively expensive for RandSVD.

4.1.2 Performance

Figure 2 compares the execution time of the two algorithms for the truncated SVD. For clarity, the figure also includes a plot showing the speed-up attained by LancSVD (with $r = 256, p = 2$) with respect to RandSVD (with $r = 16, p = 96$). The results show that LancSVD is the clear winner, with speed-up factors in the range $2\times$ to $2.5\times$ in two cases; superior to $1.2\times$ for many other problems; and below $1\times$ for 7 out of 46 matrices only.

The two top plots in Figure 2 also report the distribution of the execution time across the major building

blocks in the respective algorithms. These graphs expose that both algorithms for the truncated SVD spend a significant portion of the runtime in the SpMM routine with A^T (step S4 in LancSVD and step S3 in RandSVD) and the orthogonalization in the m -dimension (step S5 for LancSVD and step S2 for RandSVD). To put these time costs in perspective, we note that the algorithms perform exactly the same number of floating point operations (flops) in the SpMM with A and A^T , showing a clear inefficiency of this kernel in cuSPARSE when the sparse matrix is to be implicitly transposed as part of the operation and/or has more columns than rows. However, explicitly storing a transposed copy of the sparse matrix did not yield significant changes in most cases, and a few ones even exhibited much lower performance due because they present a non-zero pattern with some close-to-dense rows.

Figure 3 leverages the analytical cost models in Table 1 to further investigate the actual performance of the building blocks, showing the distribution of the theoretical flops. The plots in that figure unveil two interesting issues:

1. A significant part of flops is necessary for the orthogonalization in the m -dimension. This is in contrast with the actual execution time of this component which, as shown in Figure 2, is less dominant for many cases. Again the clear cause is the slow execution of the SpMM kernel when operating with A^T .
2. Another striking point is that RandSVD requires fewer flops than LancSVD, yet in Figure 2 the execution time of the former was reported to be considerably larger. This is due to the costly SpMM with A^T . Concretely, LancSVD with $p = 2$ performs two products of this type. In comparison, RandSVD with $r = 16, p = 96, b = 16$ involves 96 products of the same type. As a result, although RandSVD requires less flops than LancSVD, in practice the low performance of that type of kernel determines the higher execution time of the former in most cases.

The results reveal that an improved SpMM algorithm is the key to augment the performance of both RandSVD and LancSVD. This is true in particular for the case where the matrix is transposed as the cuSPARSE realization of this building block achieves only low performance. The results also reveal that, in the case of sparse problems, LancSVD is supe-

rior to RandSVD. Acknowledging the aforementioned significance of the SpMm kernel performance for the RandSVD and LancSVD implementations, a question that naturally arises is whether the LancSVD is *algorithmically* superior to RandSVD, or whether the superiority is only an artifact of the implementation of SpMm in cuSPARSE. To answer this question, we next investigate the performance of the algorithms for dense test matrices.

4.2 Dense problems

To compare the reliability and performance of RandSVD and LancSVD for dense matrices, we designed a synthetic benchmark similar to those leveraged in the literature. We set the number of columns n to 10 000 and the number of rows m to either 100 000, 250 000, 750 000 or 1 000 000. This allows us to explore the effect of a varying number of rows on performance.

The dense problems were generated using two random orthogonal matrices $X \in \mathbb{R}^{m \times n}$, $Y \in \mathbb{R}^{n \times n}$, and setting

$$A = X\Sigma Y^T, \quad (15)$$

where $\Sigma = \text{diag}(\sigma_1, \sigma_2, \dots, \sigma_n) \in \mathbb{R}^{m \times n}$ is a diagonal matrix with the desired singular values for the problem. In the experiments, we used

$$\sigma_i = \begin{cases} 10^{\frac{15i}{n/2} - 14} & \text{if } 1 \leq i \leq n/2, \quad \text{or} \\ 10^{-14} & \text{otherwise.} \end{cases} \quad (16)$$

This generates a problem where more than half of its singular values are close to zero. In addition, the singular values decay asymptotically to the rounding error ϵ in double precision.

As in our previous experiments with sparse matrices, we aim to compute 10 singular values, and set $b = 16$ as the block size. We found that, for these dense problems, a smaller size of the subspace, with $r = 64$, is enough for LancSVD to compute reasonably accurate approximations. We use two settings where we perform either one ($p = 1$) or four ($p = 4$) iterations of LancSVD. Using one LancSVD iteration, the approximation accuracy for the singular values ranges between 10^{-6} and 10^{-4} . The top plot in Figure 4 reveals that we need to perform $p = 6$ iterations of RandSVD with $r = 16$ to match this approximation accuracy. If we perform four LancSVD iterations, the approximation accuracy reaches 10^{-14} . We need to perform $p = 24$ iterations of RandSVD to

match this approximation accuracy. Thus, in both scenarios, the RandSVD needs roughly a $6\times$ higher iteration count to match the accuracy of the LancSVD. The bottom plot of Figure 4 reveals that when aiming for the same approximation quality, RandSVD is slower than LancSVD, but the speed difference between the two is smaller when the requested accuracy is low.

5 Conclusions

This work illustrates that the randomized algorithm and the block Golub-Kahan-Lanczos method for the truncated SVD can be both decomposed into a number of common basic building blocks. In addition, when the target architecture is a massively data-parallel accelerator, such as a GPU, these building blocks can be directly assembled using some orthogonalization procedures based on the Classical Gram-Schmidt and CholeskyQR algorithms. The remaining operations in the SVD algorithms comprise a few types of matrix multiplications and a couple of matrix factorizations with negligible cost. In summary, current high-performance libraries for GPUs provide the necessary numerical tools for solving low-rank approximation problems.

A second conclusion of this work is that the computational cost for the truncated algorithms is dominated, in practice, by that of matrix multiplications when operating with both dense and sparse problems. This is particularly painful for the RandSVD algorithm since, in order to obtain accurate approximations, this method requires a larger number of iterations than LancSVD and, in consequence, a larger number of matrix multiplications.

Though there may exist scenarios where the RandSVD is superior to LancSVD (in particular, when the memory capacity of system is limited), our experiments indicate that, when targeting the same approximation accuracy, LancSVD is faster than RandSVD for both dense and sparse problems.

A final remark is that the implementation of the sparse matrix multiplication in cuSPARSE, when operating with the transpose of the sparse matrix, is very slow compared with its non-transposed counterpart. This has a negative effect on LancSVD and RandSVD, but given the higher number of matrix products in the latter, its effect is more profound for that algorithm.

As part of future work, we plan to design a more sophisticated restart strategy to improve the convergence rate of the Lanczos method and, thus, reduce the num-

ber of matrix multiplications.

Acknowledgements

This work received funding from the US Exascale Computing Project (17-SC-20-SC), a collaborative effort of the U.S. Department of Energy Office of Science and the National Nuclear Security Administration; project PID2020-113656RB-C22 of MCIN/AEI/10.13039/501100011033; and the European High-Performance Computing Joint Undertaking (JU) under grant agreement No 955558 (eFlows4HPC project). The JU receives support from the European Union's Horizon 2020 research and innovation programme, and Spain, Germany, France, Italy, Poland, Switzerland, Norway.

References

- [1] Michael Anderson, Grey Ballard, James Demmel, and Kurt Keutzer. Communication-avoiding QR decomposition for GPUs. In *2011 IEEE International Parallel & Distributed Processing Symposium*, pages 48–58, 2011.
- [2] James Baglama and Lothar Reichel. Restarted block Lanczos bidiagonalization methods. *Numerical Algorithms*, 43:251–272, 11 2006.
- [3] Åke Björck. *Numerical Methods for Least Squares Problems*. Society for Industrial and Applied Mathematics, 1996.
- [4] Timothy A. Davis and Yifan Hu. The University of Florida sparse matrix collection. *ACM Transactions on Mathematical Software*, 38, 11 2011.
- [5] James Demmel, Laura Grigori, Mark Hoemmen, and Julien Langou. Communication-optimal parallel and sequential QR and LU factorizations. *SIAM Journal on Scientific Computing*, 34(1):A206–A239, 2012.
- [6] Takeshi Fukaya, Yuji Nakatsukasa, Yuka Yanagisawa, and Yusaku Yamamoto. CholeskyQR2: A simple and communication-avoiding algorithm for computing a tall-skinny QR factorization on a large-scale parallel system. In *2014 5th Workshop on Latest Advances in Scalable Algorithms for Large-Scale Systems*, pages 31–38, 2014.
- [7] Luc Giraud, Julien Langou, Miroslav Rozložník, and Jasper van den Eshof. Rounding error analysis of the Classical Gram-Schmidt orthogonalization process. *Numer. Math.*, 101(1):87–100, jul 2005.
- [8] Gene H. Golub and Charles F. Van Loan. *Matrix Computations*. The Johns Hopkins University Press, Baltimore, 3rd edition, 1996.
- [9] Gene H. Golub, Franklin T. Luk, and Michael L. Overton. A block Lanczos method for computing the singular values and corresponding singular vectors of a matrix. *ACM Trans. Math. Softw.*, 7(2):149–169, jun 1981.
- [10] Brian C. Gunter and Robert A. van de Geijn. Parallel out-of-core computation and updating the QR factorization. *ACM Trans. Math. Softw.*, 31(1):60–78, March 2005.
- [11] N. Halko, P. G. Martinsson, and J. A. Tropp. Finding structure with randomness: Probabilistic algorithms for constructing approximate matrix decompositions. *SIAM Review*, 53(2):217–288, 2011.
- [12] Eric Hallman. A block bidiagonalization method for fixed-accuracy low-rank matrix approximation. *SIAM J. Matrix Anal. Appl.*, 43(2):661–680, jan 2022.
- [13] Per-Gunnar Martinsson, Vladimir Rokhlin, and Mark Tygert. A randomized algorithm for the decomposition of matrices. *Applied and Computational Harmonic Analysis*, 30(1):47–68, 2011.
- [14] Valeria Simoncini and Daniel B. Szyld. On the occurrence of superlinear convergence of exact and inexact Krylov subspace methods. *SIAM Review*, 47(2):247–272, 2005.
- [15] Michael Yen. *An Efficient, Tolerance-Based Algorithm for the Truncated SVD*. PhD thesis, UC Berkeley, USA, 2022.